Denoising of Hyperspectral Image Using Low-Rank Matrix Factorization

Fei Xu, Yongyong Chen, Chong Peng, Yongli Wang, Xuefeng Liu, and Guoping He

***Abstract*— Restoration of hyperspectral images (HSIs) is a challenging task, owing to the reason that images are inevitably contaminated by a mixture of noise, including Gaussian noise, impulse noise, dead lines, and stripes, during their acquisition process. Recently, HSI denoising approaches based on low-rank matrix approximation have become an active research field in remote sensing and have achieved state-of-the-art performance. These approaches, however, unavoidably require to calculate full or partial singular value decomposition of large matrices, leading to the relatively high computational cost and limiting their flexibility. To address this issue, this letter proposes a method exploiting a low-rank matrix factorization scheme, in which the associated robust principal component analysis is solved by the matrix factorization of the low-rank component. Our method needs only an upper bound of the rank of the underlying low-rank matrix rather than the precise value. The experimental results on the simulated and real data sets demonstrate the performance of our method by removing the mixed noise and recovering the severely contaminated images.**

***Index Terms*— Denoising, hyperspectral image (HSI), low-rank matrix factorization.**

I. Introduction

HYPERSPECTRAL imaging has been used widely in various application fields, such as terrain classification, mineral detection and exploration, environmental monitoring, and military surveillance [1]–[3]. However, hyperspectral images (HSIs) are unavoidably corrupted by a mixture of various kinds of noise in the acquisition process, including Gaussian noise, impulse noise, dead lines, stripes, and so on. As a result, the discriminative performance of HSI is greatly degraded, and directly affects the analysis and application of images. Therefore, HSI denoising is an important and challenging research area for further analysis of images.

Till date, many denoising methods have been proposed to recover HSIs including wavelet shrinkage [4], total variation (TV) regularization [5], tensor decomposition [6], multitask sparse matrix factorization [7], sparse representation [8], and so on. More recently, HSI denoising approaches based on low-rank matrix recovery have been extensively exploited in remote sensing and achieved the state-of-the-art performance. By dividing an HSI into the overlapping patches, Zhang *et al.* [9] transformed the HSI restoration problem to a low-rank matrix recovery (LRMR) model, which was solved by an algorithm called go decomposition (GoDec) and finally removed various kinds of noise from the contaminated images. Song *et al.* [10] conducted a transform to extract the fine-image information before low-rank matrix recovery and modeled the noise removal in spectral domain as a low-rank matrix recovery problem. Unlike [9], Wang *et al.* [11] employed both the local similarity within a patch and the nonlocal similarity across the grouped patches to propose a group low-rank representation method. However, the rank of the underlying low-rank component needs to be predefined, which unfortunately is often difficult to be determined in practice.

In this letter, we exploit the low-rank property of clean HSIs and employ the robust principal component analysis (RPCA) model to reconstruct them. We solve the related model by combining the idea of patch with a novel algorithm called fast factorization proposed in our previous paper [12]. Concretely, our method can be summarized as three phases:

1) dividing an HSI into overlapped patches and lexicographically ordering each patch of the HSI into a 2-D matrix;
2) solving our model by fast factorization algorithm to derive the clean images;
3) repeating the process above and finally folding into the whole HSI.

The remainder of this letter is organized as follows. Section II presents the proposed method in detail. The experimental results are described and analyzed in Sections III and IV draws the conclusion.

II. Proposed Method

A. Low-Rank Matrix Approximation-Based Model

Based on the fact that spectral bands exhibit more relevant information with each other, a clean HSI has a low-rank property, which has been exploited in [9]. Suppose $\mathcal{D} \in \mathbf{R}^{l\times s\times n}$ is a cube of an HSI where l and s are the spatial

Manuscript received January 29, 2017; revised April 24, 2017; accepted April 27, 2017. Date of publication May 19, 2017; date of current version June 22, 2017. This work was supported in part by the National Natural Science Foundation of China under Grant 11241005 and Grant 61401244, and in part by the Science and Technology Program of the Shandong Universities of China under Grant J16LI04. *(Corresponding author: Yongli Wang.)*

F. Xu is with the College of Computer Science and Engineering, Shandong University of Science and Technology, Qingdao 266590, China, and also with the College of Mathematics and Physics, Qingdao University of Science and Technology, Qingdao 266061, China (e-mail: xf_em@163.com).

Y. Chen and Y. Wang are with the College of Mathematics and Systems Science, Shandong University of Science and Technology, Qingdao 266590, China (e-mail: YongyongChen.cn@hotmail.com; wangyongli@sdkd.net.cn).

C. Peng is with the Department of Computer Science, Southern Illinois University, Carbondale, IL 62901 USA (e-mail: pchong@siu.edu).

X. Liu is with the College of Automation and Electronics Engineering, Qingdao University of Science and Technology, Qingdao 266061, China (e-mail: nina.xf.liu@hotmail.com).

G. He is with the Shandong Academy of Sciences, Jinan 250014, China (e-mail: hegp@263.net).

Color versions of one or more of the figures in this letter are available online at http://ieeexplore.ieee.org.

Digital Object Identifier 10.1109/LGRS.2017.2700406

dimensions, and n is the spectral dimension. We first divide $\mathcal{D}$ into overlapped patches by setting the patch and step sizes, then by lexicographically ordering each patch with size of $q \times q \times n$, we can obtain a $q^2 \times n$ matrix D, which has the intrinsic low-rank property.

Therefore, a general RPCA framework [13] exploiting the "low-rank plus sparse" decomposition can be used to reconstruct the HSIs, and the model based on low-rank matrix approximation (LRMA) [9] is expressed as follows:

$$\begin{aligned} &\min_{X,Y} \ \|X\|_* + \lambda\|Y\|_1 \\ &\text{s.t. } \|D - X - Y\|_F \le \delta \end{aligned} \tag{1}$$

where $D, X, Y \in \mathbf{R}^{q^2 \times n}$, D is the observed HSI data, X is a low-rank matrix denoting the clean HSI, Y is a sparse matrix denoting non-Gaussian noise, λ is a positive regularization parameter, and $\delta > 0$ denotes the Gaussian noise level. The nuclear norm of X is defined as $\|X\|_* = \Sigma_i \sigma_i^X$, σ_i^X denotes the ith singular value of X, $\|Y\|_1$, and $\|\cdot\|_F$ denote the l_1 norm of Y and the Frobenius norm, respectively.

B. Low-Rank Matrix Factorization

The drawbacks of using nuclear norm in (1), however, are twofold: first, solving the above RPCA problem is usually an extremely time-consuming task, since the singular value decomposition (SVD) of a matrix is needed at each iteration; second, because of all the singular values being dealt with equally, the larger singular values are penalized more heavily, meaning that the nuclear norm is not a satisfactory surrogate of the rank function in real applications [14], [15]. Therefore, we exploit two strategies to overcome the above-mentioned drawbacks. First, we use $\|X\|_{\text{ld}} = \log\det(I + (X^T X)^1/2) = \sum_{i=1}^{\min\{q^2,n\}} \log(1 + \sigma_i^X)$ as the rank approximation [15] to replace the traditional nuclear norm in (1). Because $\log(1 + \sigma_i^X) \ll \sigma_i^X$ for a large $\sigma_i^X > 1$, the logdet function is a better rank approximation than the nuclear norm; second, a fast factorization $X = UCV^T$ is used so as to avoid the SVD for a large matrix. In this factorization, $U \in \mathbf{R}^{q^2 \times k}$, $C \in \mathbf{R}^{k \times k}$, $V \in \mathbf{R}^{n \times k}$, $k \ll \min\{q^2, n\}$, and $U^T U = V^T V = I$. Based on the orthogonal property of U and V, we can easily derive the following formula:

$$\begin{aligned} \|X\|_{\text{ld}} &= \log\det(I + (VC^T U^T UCV^T)^{\frac{1}{2}}) \\ &= \log\det(I + (C^T C)^{\frac{1}{2}})) = \|C\|_{\text{ld}}. \end{aligned} \tag{2}$$

In this way, our model finally reduces to the following form:

$$\begin{aligned} &\min_{C,Y,U^T U = V^T V = I} \ \|C\|_{\text{ld}} + \lambda\|Y\|_1 \\ &\text{s.t. } \|D - UCV^T - Y\|_F \le \delta. \end{aligned} \tag{3}$$

We adopt l_1 norm in the second term because [16] reveals that l_1 norm can better model non-Gaussian noise. Here, the matrix factorization provides an upper bound k for the rank of the low-rank matrix X. Therefore, we just need to determine the value of k instead of the true rank of X in advance. It is noted that [17] also uses a nonconvex rank surrogate in the form of log-determinant function, where $\log\det(X + \epsilon I) = \log\det(\Sigma^{1/2} + \epsilon I)$; additionally, [14] exploits a weighted Schatten $p-$norm to replace the nuclear norm to improve the performance of low-rank approximation; the main difference between us is that ours only needs a thin SVD of $k \times k$ matrix by matrix factorization.

C. Algorithm

We solve (3) by the augmented Lagrangian method and update the variables alternately. The augmented Lagrangian function for (3) is as follows:

$$\begin{aligned} L = \|C\|_{ld} + \lambda\|Y\|_1 + \langle D - UCV^T - Y, \Lambda\rangle \\ + \frac{\rho}{2}\|D - UCV^T - Y\|_F^2 \end{aligned} \tag{4}$$

where $\Lambda \in \mathbf{R}^{q^2 \times n}$ is the Lagrangian multiplier and ρ is the penalty parameter.

We solve (4) by the following six steps to update all the variables at each iteration.

1) *Updating Y:* The subproblem for optimizing Y is

$$\min_Y \frac{1}{2}\|Y - \Theta\|_F^2 + \frac{\lambda}{\rho}\|Y\|_1 \tag{5}$$

where $\Theta = D - UCV^T + (1/\rho)\Lambda$, by performing the elementwise soft-thresholding operators [18] on Y, we have

$$Y_{\text{ij}} = \text{sign}(\Theta_{ij})\max\left(\Theta_{\text{ij}} - \frac{\lambda}{\rho}, 0\right). \tag{6}$$

2) *Updating U:* The subproblem for optimizing U is

$$\min_{U^T U = I} \|UC - \Gamma V\|_F^2 \tag{7}$$

where $\Gamma = D - Y + (1/\rho)\Lambda$, by resorting to the classical orthogonal Procrustes problem [19], we have

$$U = \mathcal{L}(\Gamma VC^T)(\mathcal{R}(\Gamma VC^T))^T \tag{8}$$

where $\mathcal{L}(Z)$ and $\mathcal{R}(Z)$ are the left and right singular vectors of Z, respectively.

3) *Updating V:* Similar to 2), we have

$$V = \mathcal{L}(\Gamma^T UC)(\mathcal{R}(\Gamma^T UC))^T. \tag{9}$$

4) *Updating C:* Optimizing C is to solve the following subproblem

$$\min_C \|C\|_{ld} + \frac{\rho}{2}\|U^T \Gamma V - C\|_F^2 \tag{10}$$

by using the singular value shrinkage operator [20]

$$C = \mathcal{F}_{\frac{1}{\rho}}(U^T \Gamma V) \tag{11}$$

where $\mathcal{F}_\tau(Z) = \mathcal{L}(Z)\text{diag}(\max(0, \sigma_i^Z - \tau))\mathcal{R}(Z)^T$.

5) *Updating Λ and ρ:* By the standard updating way, we have

$$\Lambda = \Lambda + \rho(D - UCV^T - Y), \quad \rho = \beta * \rho \tag{12}$$

where $\beta > 1$ is a constant and controls the convergence speed.

The stopping criterion of our algorithm is the root mean square error being less than 10^{-3}, namely, $\|D - UCV^T - Y\|_F / \|D\|_F \leq 10^{-3}$. Combining the three phases of our method aforementioned in Section I, we summarize all the details in Algorithm 1.

Algorithm 1 HSI Denoising via Fast Matrix Factorization

Require: Original HSI $\mathcal{D} \in \mathbf{R}^{l \times s \times n}$

Ensure: Clean HSI $\mathcal{X} \in \mathbf{R}^{l \times s \times n}$

Step 1: Divide $\mathcal{D}$ into patches and lexicographically order each patch to obtain a matrix $D \in \mathbf{R}^{q^2 \times n}$;

Step 2: Recover the low-rank component X from D by using the matrix factorization technique in (3);

Step 3: Reconstruct HSI $\mathcal{X}$ by repeating **Step 2** for each patch, averaging the overlapped parts and folding them together.

Considering that $k \ll \min\{q^2, n\}$, our algorithm has complexity $O(nq^2k)$ by omitting the high-order terms of k. In addition, the other two compared low-rank based denoising methods LRMR [9] and noise adjusted iterative LRMA (NAILRMA) [21] in our experiment, which utilize the GoDec algorithm and the randomized SVD (RSVD) algorithm respectively to solve the related optimization problems, need $O(nq^2k)$ flops and $O(q^2n\log(k) + (q^2 + n)k^2)$ flops correspondingly [9], [21], where k is the upper bound of the rank of the low-rank matrix. In view of the computational complexity, for each iteration, our method is comparable with LRMR, but slightly higher than NAILRMA. However, the better rank approximation in our method leads to less iteration steps so as to improve the computation time (see Table II in Section III-C).

III. Experimental Results and Discussion

To verify the effectiveness of the proposed method, we compare our method with several state-of-the-art algorithms, including video block matching 3-D filtering (VBM3D) [22], LRMR [9], and NAILRMA [21]. It is noted that the last two methods are recently developed methods, which ensures comparison with the latest advancements in this area.

A. Simulated Data Experiment

The Hyperspectral Digital Imagery Collection Experiment image of the Washington DC Mall[1] is used in our simulated experiment. The selected image size is $150 \times 150 \times 163$. In our simulated experiment, several kinds of noise are added to the Washington DC image.

1) We randomly add zero-mean Gaussian noise to all the bands of the image. The signal-to-noise (SNR) value of each band varies from 20 to 30 dB, and the mean SNR value of all the bands is 24.83 dB.
2) We randomly add impulse noise to all the bands of the image. The percentage of impulse noise is 20%. The noise density of each band varies from 0.1 to 0.2, and the mean noise density of all the bands is 0.1466.
3) Dead lines and stripes are simulated for bands 70 and 111, respectively.

[1]https://engineering.purdue.edu/~biehl/MultiSpec

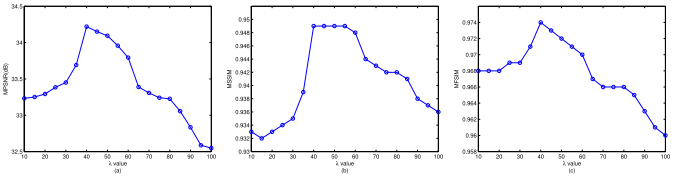

Fig. 1. Sensitivity analysis of regularization parameter λ (λ value from 10 to 100). (a) Change in the MPSNR value. (b) Change in the MSSIM value. (c) Change in the MFSIM value.

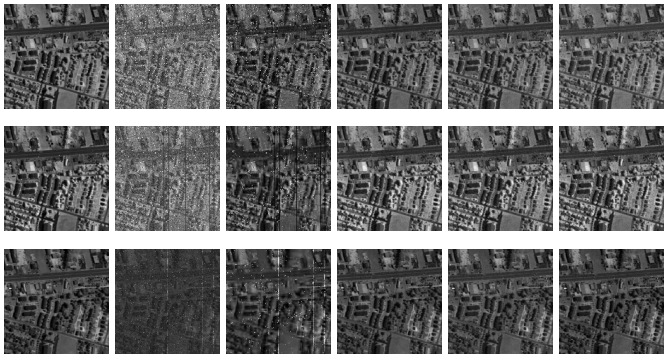

Fig. 2. Mixed-noise removal results on simulated data: Washington DC Mall. (Top to bottom) Results for bands 100, 70, and 111, which include Gaussian and impulse noise only, these two kinds and dead lines, and these two kinds and stripes, respectively. (Left to right) Clean images, noisy images, and the restored images obtained by VBM3D, LRMR, NAILRMA, and ours, respectively. This figure can be better viewed in a zoomed-in PDF.

The parameters are set as: the patch size is 20, the step size is 8, $k = 5$, $\lambda = 40$, $\rho = 0.05$ and $\beta = 1.5$. All the competing algorithms are used by default parameters.

As shown in [12], small k is usually effective enough. Hence, we use a similar strategy and tune k with small values in the set {4–7}, which turns out to have insensitive effects on the final denoising performance. To investigate how λ affects the denoising performance, we vary λ from 10 to 100 and show the performance in three measures in Fig. 1. It is seen that the proposed method has very competitive performance with a broad range of λ values, revealing the insensitivity of the proposed method to parameter. Its insensitivity suggests its potential in real-world applications.

Fig. 2 presents the restoration results of the four algorithms; it can be clearly observed that VBM3D causes the result to be oversmooth and fails to restore the image in some regions, while the other three have similar visual results, effectively suppress the Gaussian noise and impulse noise, and remove all the dead lines and stripes.

For further comparison, we also compute the mean values of the peak SNR (PSNR), structural similarity (SSIM) [23] and feature similarity (FSIM) [24], which are denoted as MPSNR, MSSIM, and MFSIM, respectively. We show these results in Table I. It can be observed that all the mean values obtained by our method are higher than those of the other three methods, demonstrating the advantage of our proposed method over the others.

TABLE I

QUANTITATIVE EVALUATION OF THE DIFFERENT RESTORATION METHODS ON THE SIMULATED DATA

Method	Noisy	VBM3D	LRMR	NAILRMA	Ours
MPSNR	17.095	20.622	33.216	33.604	**34.220**
MSSIM	0.368	0.544	0.945	0.942	**0.949**
MFSIM	0.723	0.812	0.966	0.969	**0.974**

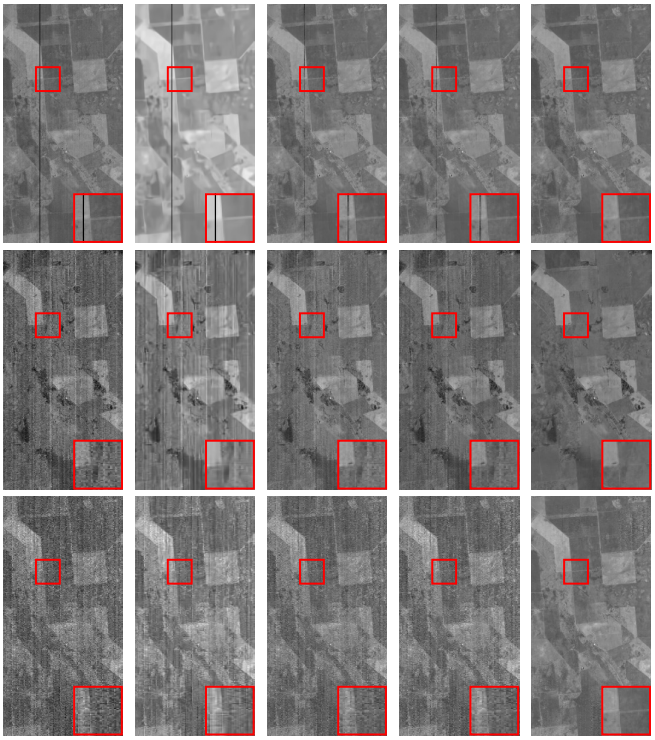

Fig. 3. Restoration results on real data: EO-1 Hyperion Australia. (Top to bottom) Images located at bands 61, 88, and 51. (Left to right) Original images and restored images obtained by VBM3D, LRMR, NAILRMA, and ours, respectively. This figure can be better viewed in the zoomed-in PDF.

B. Real Data Experiment

EO-1 Hyperion Australia data set[2] with the original size of $3858 \times 256 \times 242$ is selected for our real data experiment. Similar to [14], after removing the overlapping bands between visual near-infrared and shortwave infrared ranges, the final test image is cut to the size of $400 \times 200 \times 150$ in our experiment. The parameters are set as: the patch size is 50, the step size is 16, $k = 5$, $\lambda = 100$, $\rho = 0.05$, and $\beta = 1.5$. All the competing algorithms are used by default parameters.

Fig. 3 presents the denoising results at bands 61, 88, and 51 under slight, moderate, and severe noise levels, respectively, all of which contain dead lines and stripes. Obviously, the VBM3D algorithm still causes oversmooth results and fails to restore images under moderate and heavy noise levels. Note that the major advantage of our algorithm is centralized on the performance of removing dead lines and stripes. In detail, when handling the dead lines, our proposed method outperforms all the compared methods, which leads to the remaining ghost shadow more or less at band 61, as shown in the first row of Fig. 3; additionally, almost all the stripes are suppressed by using our method, however, the methods LRMR and NAILRMA can only partly remove them, as illustrated in the last two rows of Fig. 3 (see the zoomed-in windows on the bottom-right corner of each subfigure).

[2]http://remote-sensing.nci.org.au/

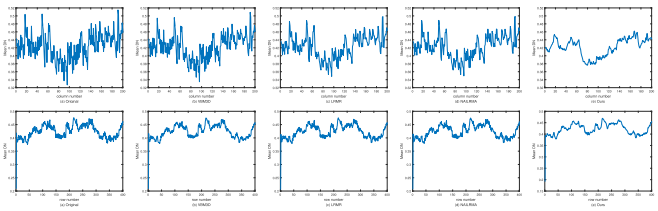

Fig. 4. Vertical and horizontal mean profiles of band 51 before and after denoising in EO-1 Hyperion Australia data set. (Top to bottom) Vertical mean profiles and horizontal mean profiles, respectively. (Left to right) Original image and the restored images obtained by VBM3D, LRMR, NAILRMA, and ours, respectively. This figure can be better viewed in the zoomed-in PDF.

TABLE II

COMPARISONS OF RUNNING TIME (IN SECONDS) FOR THE HSI DENOISING APPROACHES ON DATA SETS

Model	VBM3D	LRMR	NAILRMA	Ours
Washington DC Mall	59.372	855.692	110.363	**39.857**
Australia Data Set	105.94	1116.15	**73.76**	148.20

Fig. 4 shows the vertical and horizontal mean profiles of band 51 before and after denoising. For the vertical mean profiles, the vertical axis represents the mean digital number (DN) values of each column and the horizontal axis shows the column number, similarly, the row for the horizontal mean profiles. The first curve in Fig. 4 has rapid fluctuations due to the existence of stripes. Compared to the other three, our algorithm provides smoother curves indicating that the stripes can be removed more effectively.

C. Running Time

We have compared the running time of all methods and shown the results in Table II. It is seen that our method has at least comparable, if not the best, speed over the other methods. Realizing that our method has better denoising capability, this efficiency implies the high potential of our method in real-world applications.

IV. CONCLUSION

In this letter, we propose a denoising method based on the low-rank scheme and solve the associated model by the fast matrix factorization, which avoids the computationally expensive SVD, unlike the traditional methods using the nuclear norm as the convex rank approximation. Another advantage of our method is that different from the other LRMA-based methods, the rank of the low-rank matrix does not need to be determined, because we may set the upper bound of the rank of this low-rank matrix to be a small integer. The experimental results on simulated and real data sets confirm that our proposed method has advantage over

the other compared methods in removing the mixed noise effectively and efficiently.

REFERENCES

[1] Y.-Q. Zhao and J. Yang, "Hyperspectral image denoising via sparse representation and low-rank constraint," *IEEE Trans. Geosci. Remote Sens.*, vol. 53, no. 1, pp. 296–308, Jan. 2015.

[2] L. Zhang, L. Zhang, D. Tao, X. Huang, and B. Du, "Compression of hyperspectral remote sensing images by tensor approach," *Neurocomputing*, vol. 147, no. 1, pp. 358–363, Jan. 2015.

[3] C. Li, Y. Ma, J. Huang, X. Mei, and J. Ma, "Hyperspectral image denoising using the robust low-rank tensor recovery," *J. Opt. Soc. Amer. A*, vol. 32, no. 9, pp. 1604–1612, Sep. 2015.

[4] H. Othman and S.-E. Qian, "Noise reduction of hyperspectral imagery using hybrid spatial-spectral derivative-domain wavelet shrinkage," *IEEE Trans. Geosci. Remote Sens.*, vol. 44, no. 2, pp. 397–408, Feb. 2006.

[5] H. Zhang, "Hyperspectral image denoising with cubic total variation model," *SPRS Ann. Photogramm., Remote Sens. Spatial Inf. Sci.*, vol. I-7, pp. 95–98, Jul. 2012.

[6] X. Guo, X. Huang, L. Zhang, and L. Zhang, "Hyperspectral image noise reduction based on rank-1 tensor decomposition," *ISPRS J. Photogramm. Remote Sens.*, vol. 83, no. 9, pp. 50–63, Sep. 2013.

[7] M. Ye, Y. Qian, and J. Zhou, "Multitask sparse nonnegative matrix factorization for joint spectral–spatial hyperspectral imagery denoising," *IEEE Trans. Geosci. Remote Sens.*, vol. 53, no. 5, pp. 2621–2639, May 2015.

[8] J. Ma, J. Zhao, J. Tian, X. Bai, and Z. Tu, "Regularized vector field learning with sparse approximation for mismatch removal," *Pattern Recognit.*, vol. 46, no. 12, pp. 3519–3532, Dec. 2013.

[9] H. Zhang, W. He, L. Zhang, H. Shen, and Q. Yuan, "Hyperspectral image restoration using low-rank matrix recovery," *IEEE Trans. Geosci. Remote Sens.*, vol. 52, no. 8, pp. 4729–4743, Aug. 2014.

[10] H. Song, G. Wang, and K. Zhang, "Hyperspectral image denoising via low-rank matrix recovery," *Remote Sens. Lett.*, vol. 5, no. 10, pp. 872–881, Oct. 2014.

[11] M. Wang, J. Yu, J.-H. Xue, and W. Sun, "Denoising of hyperspectral images using group low-rank representation," *IEEE J. Sel. Topics Appl. Earth Observ. Remote Sens.*, vol. 9, no. 9, pp. 4420–4427, Sep. 2016.

[12] C. Peng, Z. Kang, and Q. Chen. "A fast factorization-based approach to robust PCA." Unpublished paper, 2016. [Online]. Available: https://arxiv.org/pdf/1609.08677.pdf

[13] J. Wright, A. Ganesh, S. Rao, Y. Peng, and Y. Ma, "Robust principal component analysis: Exact recovery of corrupted low-rank matrices via convex optimization," in *Proc. Adv. Neural Inf. Process. Syst.*, Vancouver, BC, Canada, Dec. 2009, pp. 2080–2088.

[14] Y. Xie, Y. Qu, D. Tao, W. Wu, Q. Yuan, and W. Zhang, "Hyperspectral image restoration via iteratively regularized weighted schatten p-norm minimization," *IEEE Trans. Geosci. Remote Sens.*, vol. 54, no. 8, pp. 4642–4659, Aug. 2016.

[15] C. Peng, Z. Kang, M. Yang, and Q. Cheng, "Feature selection embedded subspace clustering," *IEEE Signal Process. Lett.*, vol. 23, no. 7, pp. 1018–1022, Jul. 2016.

[16] J. Ma, C. Chen, C. Li, and J. Huang, "Infrared and visible image fusion via gradient transfer and total variation minimization," *Inf. Fusion*, vol. 31, pp. 100–109, Sep. 2016.

[17] W. Dong, G. Shi, X. Li, Y. Ma, and F. Huang, "Compressive sensing via nonlocal low-rank regularization," *IEEE Trans. Image Process.*, vol. 23, no. 8, pp. 3618–3632, Aug. 2014.

[18] D. L. Donoho, "De-noising by soft-thresholding," *IEEE Trans. Inf. Theory*, vol. 41, no. 3, pp. 613–627, May 1995.

[19] P. H. Schönemann, "A generalized solution of the orthogonal Procrustes problem," *Psychometrika*, vol. 31, no. 1, pp. 1–10, Mar. 1966.

[20] J.-F. Cai, E. J. Candes, and Z. Shen, "A singular value thresholding algorithm for matrix completion," *SIAM J. Optim.*, vol. 20, no. 4, pp. 1956–1982, 2010.

[21] W. He, H. Zhang, L. Zhang, and H. Shen, "Hyperspectral image denoising via noise-adjusted iterative low-rank matrix approximation," *IEEE J. Sel. Topics Appl. Earth Observ. Remote Sens.*, vol. 8, no. 6, pp. 3050–3061, Jun. 2015.

[22] K. Dabov, A. Foi, V. Katkovnik, and K. Egiazarian, "Image denoising by sparse 3-D transform-domain collaborative filtering," *IEEE Trans. Image Process.*, vol. 16, no. 8, pp. 2080–2095, Aug. 2007.

[23] Z. Wang, A. C. Bovik, H. R. Sheikh, and E. P. Simoncelli, "Image quality assessment: From error visibility to structural similarity," *IEEE Trans. Image Process.*, vol. 13, no. 4, pp. 600–612, Apr. 2004.

[24] L. Zhang, L. Zhang, X. Mou, and D. Zhang, "FSIM: A feature similarity index for image quality assessment," *IEEE Trans. Image Process.*, vol. 20, no. 8, pp. 2378–2386, Aug. 2011.